Effects of Moist Froude Number and CAPE on a Conditionally Unstable Flow over a Mesoscale Mountain Ridge

SHU-HUA CHEN

Department of Land, Air, and Water Resources, University of California, Davis, Davis, California

YUH-LANG LIN

Department of Marine, Earth, and Atmospheric Sciences, North Carolina State University, Raleigh, North Carolina

ABSTRACT

In this study, idealized simulations are performed for a conditionally unstable flow over a two-dimensional mountain ridge in order to investigate the propagation and types of cloud precipitation systems controlled by the unsaturated moist Froude number (F_w) and the convective available potential energy (CAPE). A two-dimensional moist flow regime diagram, based on F_w and CAPE, is proposed for a conditionally unstable flow passing over a two-dimensional mesoscale mountain ridge. The characteristics of these flow regimes are 1) regime I: flow with an upstream-propagating convective system and an early, slowly moving convective system over the mountain; 2) regime II: flow with a long-lasting orographic convective system over the mountain peak, upslope, or lee slope; 3) regime III: flow with an orographic convective or mixed convective and stratiform precipitation system over the mountain and a downstream-propagating convective system; and 4) regime IV: flow with an orographic stratiform precipitation system over the mountain and possibly a downstream-propagating cloud system. Note that the fourth regime was not included in the flow regimes proposed by Chu and Lin and Chen and Lin. The propagation of the convective systems is explained by the orographic blocking and density current forcing associated with the cold-air outflow produced by evaporative cooling acting against the basic flow, which then determines the propagation and cloud types of the simulated precipitation systems.

---

1. Introduction

Understanding the formation and propagation of precipitation systems in the vicinity of mesoscale mountains is essential in helping forecast orographic rain and the damages caused by flooding associated with it. The propagation of orographic precipitation systems may be controlled by various factors, such as the basic wind speed (U), moist Brunt–Väisälä frequency (N_w), mountain height (h) and width, convective available potential energy (CAPE), atmospheric moisture content, and vertical wind shear. Based on idealized numerical simulations, Chu and Lin (2000; hereafter CL) identified three moist flow regimes for a two-dimensional conditionally unstable flow over a mesoscale mountain ridge: 1) regime I: flow with an upstream-propagating convective system; 2) regime II: flow with a quasi-stationary convective system over the mountain peak; and 3) re-

gime III: flow with both a quasi-stationary convective system over the mountain peak and a downstream-propagating convective system. They proposed that the unsaturated moist Froude number $F_w = U/N_w h$ might serve as the control parameter for these flow regimes. In regime I (with low F_w), the quasi-continuous and heavy rainfall is produced over the upslope side of the terrain and adjacent plains as individual convective cells develop farther upstream at the head of the density current. The convective cells then propagate downstream once they form. In regime II (with moderate or critical F_w), the convective system becomes quasi-stationary over the upslope side of the terrain and in the vicinity of the mountain peak. A balance between the momentum forcing associated with the basic flow and the forcing associated with the cold-air outflow is reached in this flow regime. In regime III (with large F_w), two convective system modes are identified: a quasi-stationary convective system over the mountain ridge and a downstream-propagating convective system. For the quasi-stationary convective system located over the mountain, the formation mechanisms are the same as those for regime II. For the downstream-

Corresponding author address: Dr. Shu-Hua Chen, Department of Land, Air, and Water Resources, University of California, Davis, One Shields Avenue, Davis, CA 95616.
E-mail: shachen@ucdavis.edu

propagating convective system, the convective cells are mainly generated by the convergence at the front edge of the downslope wind, which is located over the lee slope.

Chen and Lin (2004) found that the flow regimes identified by CL also exist in a three-dimensional conditionally unstable flow. In their study, the moist Brunt–Väisälä frequency was defined as $N_w^2 = (g/\theta_v)\partial\theta_v/\partial z$ (e.g., see Emanuel 1994), where θ_v is the virtual potential temperature and g is the acceleration of gravity, for moist but unsaturated air in order to avoid negative values. In addition, they found that heavy orographic rainfall might be produced under a strong incoming flow and that the quasi-stationary convective system tends to be located over the upslope side of the terrain, which is more consistent with observations (e.g., see the brief review provided by Lin et al. 2001b). Miglietta and Buzzi (2001) studied the role of moisture in flow regime transitions, namely between "flow over" and "flow around" a mesoscale mountain. They found that moist processes favor the flow over regime, instead of the flow-around regime. However, Stein (2004) argued that this conclusion is less evident for a conditionally unstable flow because the air is under the influence of either the dry, moist, or even the negative Brunt–Väisälä frequency, depending on the saturation state. Schneidereit and Schär (2000) showed that, if an east–west oriented, idealized Alpine mountain ridge has a western flank (i.e., the existence of a concave geometry), the flow in the presence of a finite-width southerly jet can undergo transitions between the "go around" and "go over" regimes. In studying the 1994 Piedmont flood, Rotunno and Ferretti (2001) found that these flow regimes are also influenced by the horizontal moisture gradient. By comparing the results of Miglietta and Buzzi (2001) with Chen and Lin (2004), it appears that the three-dimensional flow-around regime corresponds to regime I as classified by CL, while the flow-over regime corresponds to either CL's regime II or III. In exploring convective flow regimes over real Alpine topography, Stein (2004) also found the existence of regime II for a conditionally unstable sounding observed at Cagliari, Sardinia, during the Mesoscale Alpine Program (MAP; see Binder and Schär 1996; Bougeault et al. 2001) Intensive Observation Period-2 (IOP-2). In other words, the three-dimensional flow regimes are also controlled by the unsaturated moist Froude number.

Although F_w may serve as an effective control parameter for the propagation of orographic precipitation, it may not completely represent some flow characteristics, especially when the incoming airstream is conditionally unstable. For example, the CAPE associated with a conditionally unstable airstream might be released if the orographic forcing is sufficiently large to lift the incoming air parcels in the boundary layer above the level of free convection (LFC). Under this situation, CAPE will be released, resulting in the acceleration of the air parcels upward, which can then generate and/or strengthen the convective systems over the mountain and its surrounding area. To understand the formation and distribution of orographic rain, we hypothesize that CAPE can influence the classification of moist flow regimes, and it may serve as a control parameter, in addition to F_w. This hypothesis is also consistent with the ingredient argument recently proposed by Lin et al. (2001a).

In fact, the preliminary numerical experiments of two-dimensional (Chu and Lin 1998) and three-dimensional (Chen and Lin 2004) flow have shown that flow regimes tend to shift from higher number regimes to lower number regimes when the CAPE is large. For example, regime II (III) would shift to regime I (II) when the CAPE is large and the flow regimes are defined as in CL. CAPE has also been found to play important roles in producing orographic rainfall over the Alps (e.g., Lin et al. 2001b; Stein 2004). By varying CAPE and convective inhibition (CINH), Stein (2004) found a flow in which no convection develops. Rather, only stratiform rain, in which the cloud depth is less than 4 km, is produced when CAPE and CINH are equal to -200 and 400 J kg^{-1}, respectively (e.g., their case M3K20). However, more rainfall is produced, and some convection is triggered away from the center of the arc of the Alps. To understand the formation and propagation of orographic rain more thoroughly, the complex dynamics of the flow behavior needs to be further explored by taking a systematic approach and performing numerical experiments using idealized soundings and mountain geometries.

This paper is organized as follows: The numerical model is described and our experimental designs are presented in section 2. Results of idealized numerical simulations are then discussed in section 3, which includes verification of the model, effects of CAPE, and discussion of the regime diagram based on our two chosen control parameters, F_w and CAPE. Concluding remarks are then made in section 4.

2. Model description and experiment design

The Weather Research and Forecast (WRF) model is a next-generation mesoscale model developed by a group of scientists from different institutions and research centers (Chen and Dudhia 2000; Michalakes et al. 2001; Skamarock et al. 2001). WRF is a fully compressible, three-dimensional (3D) nonhydrostatic model, and the governing equations are written in flux form. The terrain-following height coordinate $(\sigma - z)$ is used for this study. The Runge–Kutta third-order time scheme and fifth- and third-order advection schemes are adopted in the horizontal and vertical directions, respectively (Wicker and Skamarock 2002). An open (radiative) lateral boundary condition in the north–south direction, a free-slip lower boundary condition,

and a periodic boundary condition in the east–west direction are also chosen. The Purdue–Lin (Chen and Sun 2002) microphysics parameterization scheme is activated in all simulations, which is based on Lin et al. (1983) and Rutledge and Hobbs (1984) with some modifications, and the equivalent ice potential temperature is treated as a conserved variable. (Detailed information about the WRF model is available online at www.wrf-model.org.)

The horizontally homogeneous initial conditions are from Schlesinger (1978) with specified wind fields, and the sounding of the control case (CNTL) has a CAPE about 3000 J kg^{-1}, which is calculated from the following formula:

$$\text{CAPE} = \int_{z_1}^{z_2} \frac{g(\theta_p - \theta)}{\theta}\, dz, \qquad (1)$$

where z_1 and z_2 are the LFC and level of neutral buoyancy (LNB), respectively, g (=9.8 m s^{-1}) is gravitational acceleration, θ the potential temperature of the sounding (environment), and θ_p is the potential temperature of an air parcel that is lifted from mixed air at the lowest 500 m. The tropopause of this sounding is located at approximately 12 km, and the atmosphere above this level is assumed to be isothermal up to the upper boundary (i.e., 20 km). The *unsaturated* moist Brunt–Väisälä frequency (N_w) is approximately 0.0095 s^{-1}, which is estimated from the surface to approximately 3 km in a column away from the mountain ridge based on the following formula (Emanuel 1994):

$$N_w^2 = \frac{g}{\overline{\theta}_v} \frac{\partial \theta_v}{\partial z}, \qquad (2)$$

where θ_v is the virtual potential temperature and $\overline{\theta}_v$ is the mean virtual potential temperature in the layer considered. A uniform southerly flow and temperature profile are imposed across the entire model domain. However, different basic wind speeds and temperature profiles are also tested for different cases.

In this study, idealized, two-dimensional mountain geometry is used with the formula for the surface terrain (h_{sfc}) as

$$h_{\text{sfc}} = \frac{h}{1 + [(x - x_o)/a]^2}. \qquad (3)$$

The parameters for the mountain height (h), half-width (a), and horizontal grid spacing (Δx) in the model are 2, 30, and 1 km, respectively, and are kept constant throughout in this study. The horizontal domain has 1001 grid points, which spans a physical length of 1000 km. The vertical grid interval is stretched from 30 m at the lowest model level to 500 m near the domain top. There are 50 vertical levels in the model, yielding a physical domain height of 20 km. A 5-km-deep sponge

layer is added to the upper part of the physical domain to reduce artificial wave reflection. The mountain is introduced impulsively into the basic flow at the time the simulation is started, that is, $t = 0$ s. For all cases, the model time step is 1 s and the model is integrated for 10 h.

The CNTL (also called CP4F2) experiment uses a basic southerly wind of $U = 5$ m s^{-1}, which gives $F_w = 0.262$, and the thermodynamic sounding from Schlesinger (1978; Fig. 1), which gives a CAPE of about 3000 J kg^{-1}. To investigate the effects of F_w and CAPE on a conditionally unstable flow over a mesoscale mountain, a matrix of numerical experiments is conducted based on two control parameters, F_w and CAPE. Cases with different F_w are based on the variation of U and are denoted by (F1, F2, F3, F4, F5, F6) = (0.131, 0.262, 0.524, 0.786, 1.048, 1.572), which correspond to $U = $ (2.5, 5, 10, 15, 20, 30 m s^{-1}), respectively. Note that variation of F_w may also be accomplished by varying other dimensional parameters, such as h and N_w. In this study, however, we choose to take the same approach as that of CL by only varying U and keeping h and N_w constant. This is necessary as the second nondimensional control parameter, related to CAPE, may be influenced by variations in h, U, or N_w. The mountain half-width is also kept at a constant of 30 km for all cases. Cases with different CAPE are based on the variation of temperature profile above 2.0 km (see Fig.
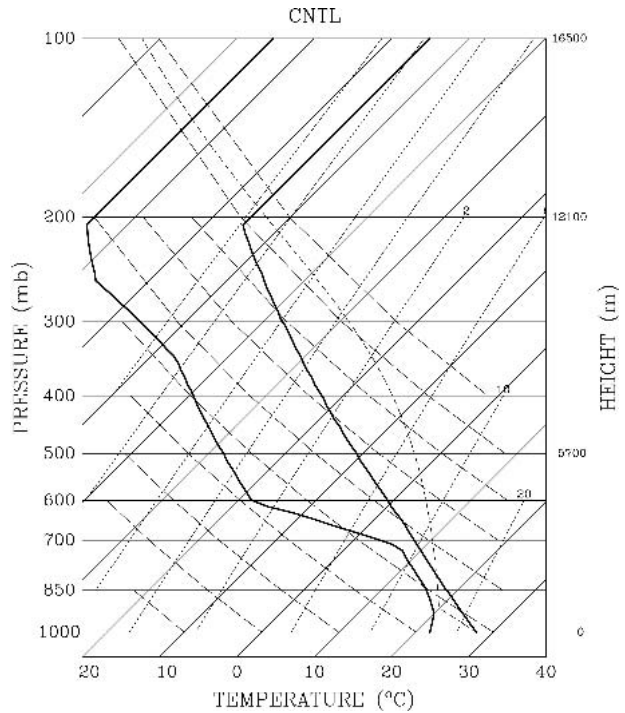

FIG. 1. The sounding for the CNTL case, which is identical to that of Schlesinger (1978). The sounding has a CAPE about 3000 J kg^{-1}. The wind is assumed uniform with height and a speed of 5 m s^{-1}.

9), in order to keep the low-level CINH constant. This variation is denoted by CP0, CP1, CP2, CP3, CP4, and CP5 and correspond to CAPE = 487, 1372, 1895, 2438, 3000, and 3578, respectively. The formulas for modifications of those temperature soundings are as follows:

$$\begin{cases} T' = 0, & z \leq z_b \\ T' = \min(T_{pturb}, T_{pturb}(z - z_b)/z_{ref}), & z > z_b \end{cases}, \quad (4)$$

where T' is the modification, $z_b = 2$ km, $z_{ref} = 5$ km, and z is the height measured in km. For cases CP0F2, CP1F2, CP2F2, CP3F2, and CP5F2, $T_{pturb} = 9, 6, 4, 2$, and -2, respectively. The basic flow parameters for a subset of numerical experiments, to be discussed in more detail in the text, and their associated flow regimes are summarized in Table 1. A more complete set of experiments, based on two control parameters, F_w and CAPE, is conducted, and a moist flow regime diagram is then proposed.

3. Results

a. Verification of the model and effects of F_w

To verify the model, we perform numerical simulations with various unsaturated moist Froude numbers by changing the basic flow speeds and then compare the results with the 2D flow regimes proposed by CL. Figures 2a and 2b show the vertical velocity and potential temperature fields for the control (CNTL/CP4F2) case after $t = 3$ h and $t = 7$ h, respectively, for a uniform, conditionally unstable flow over a two-dimensional mountain ridge with $h = 2$ km, $a = 30$ km, and $U = 5$ m s^{-1}. The unsaturated moist Froude number (F_w) is 0.262. The convective system is initiated at the peak of the mountain. During the first 3 h of the simulation, the slowly moving system remains in the vicinity of the mountain peak with more convective cells located on the lee side (Fig. 2a) where the maximum accumulated

rainfall is located (Fig. 3). After $t = 3$ h, new convective cells start to develop upstream of the convective system, which propagates slowly away from the mountain (Fig. 2b). The movement of the system can be seen from the temporal evolution of the vertical velocity at a height of 3.6 km in Fig. 3. At a later time ($t = 8$ h) until the end of simulation, the system becomes much weaker ($w \approx 4$ m s^{-1}), and the rainfall becomes very light.

The upstream-propagating convective system is primarily generated by the low-level convergence associated with the upstream-propagating density current that is produced by evaporative cooling. According to CL, this flow belongs to regime I in which a slowly moving, strong convective system develops early in the vicinity of the mountain peak and subsequently propagates upstream. We therefore propose regime I of CL be *modified to include an early, slowly moving convective system* in the vicinity of the mountain peak in addition to the upstream-propagating convective system. Note that a weak convective cell associated with light rainfall appears to be produced by the shallow downstream-propagating density current, which travels downstream rather rapidly at a speed of about 11 m s^{-1}. From Fig. 3, it can be seen that this weak convective cell is not produced numerically by the initial shock; rather, it is produced physically by the low-level convergence associated with the density current generated by the evaporative cooling associated with the precipitation of the convective system at about $t = 1$ h.

As shown in Fig. 2a, the air is warmed by either the latent heat generated by the upward motion inside the deep convective cells or by adiabatic warming associated with the weak, compensated downward motion between the deep convective cells. Due to the subsidence warming, the diabatic heating coincides better with the vertical velocity (Fig. 4a) than with potential temperature perturbation (Fig. 4b). It appears that two convective cell modes exist during the simulation,

TABLE 1. Flow parameters of the CAPE, basic wind (U), the equivalent vertical velocity (W_{max}), the unsaturated moist Brunt–Väisälä frequency (N_w), and the unsaturated moist Froude number (F_w) for some cases and their associated flow regimes. $W_{max} = \sqrt{2CAPE}$, $N_w = (g/\theta_v)\partial\theta_v/\partial z$, $F_w = U/(N_w h)$, and $h = 2$ km in all cases except $h = 1$ km in CP4F6. Cases are named as follows: CP0, CP1, CP2, CP3, CP4, and CP5 mean CAPE = 487, 1372, 1895, 2438, 3000, and 3578 J kg^{-1}, respectively; F1, F2, F3, F4, F5, and F6 mean $F_w \approx$ 0.131, 0.262, 0.524, 0.786, 1.048, and 1.572, respectively.

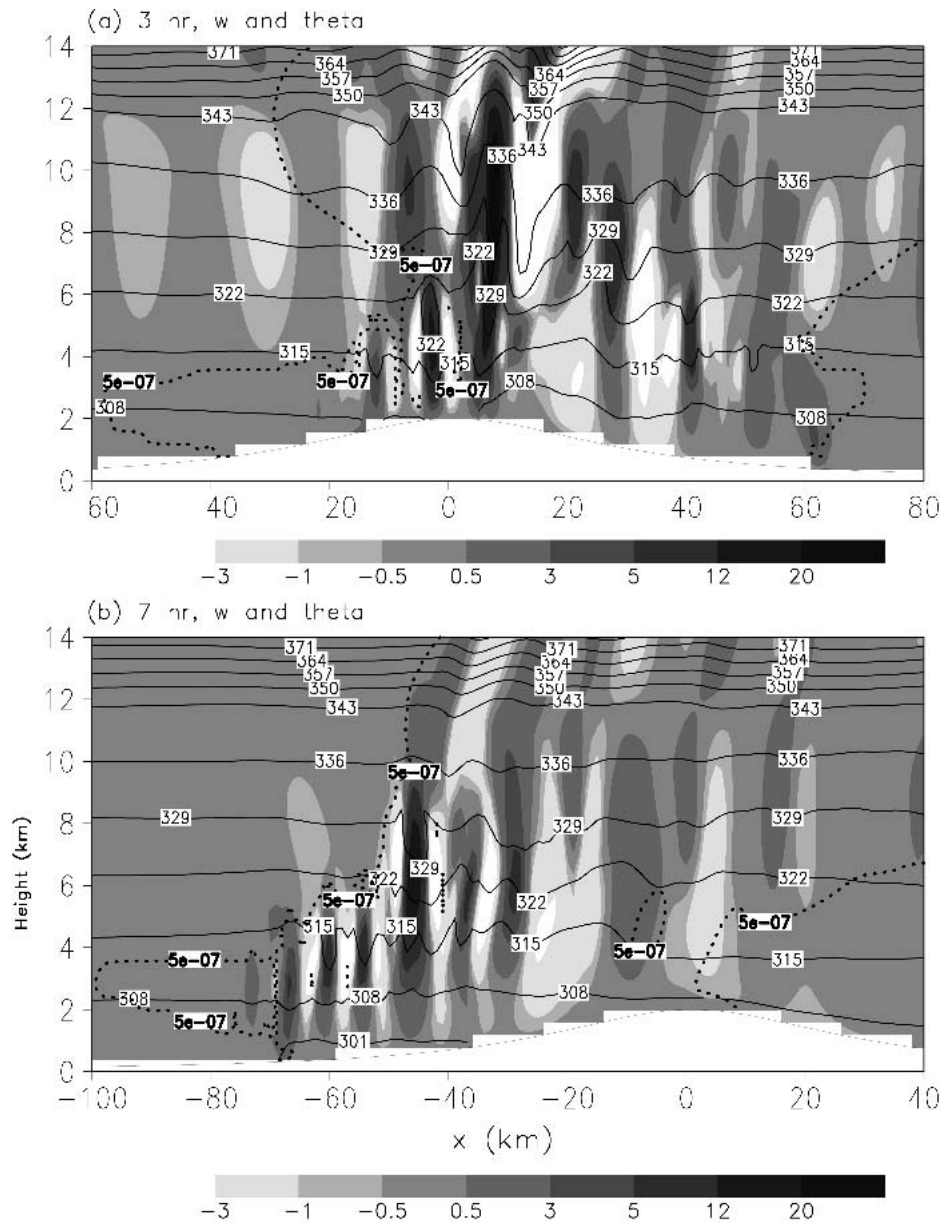|	CAPE (J kg^{-1})	U (m s^{-1})	W_{max} (m s^{-1})	N_w (s^{-1})	F_w	Regime
CNTL (CP4F2)	3000	5	77.5	9.54×10^{-3}	0.262	I
CP4F1	3000	2.5	77.5	9.54×10^{-3}	0.131	I
CP4F3	3000	10	77.5	9.54×10^{-3}	0.524	II
CP4F4	3000	15	77.5	9.54×10^{-3}	0.786	III
CP4F5	3000	20	77.5	9.54×10^{-3}	1.048	IV
CP4F6	3000	30	77.5	9.54×10^{-3}	1.572	IV
CP0F2	487	5	31.2	1.01×10^{-2}	0.250	IV
CP1F2	1372	5	52.4	9.75×10^{-3}	0.256	II
CP2F2	1895	5	61.6	9.69×10^{-3}	0.258	II
CP3F2	2438	5	69.8	9.62×10^{-3}	0.260	II
CP5F2	3578	5	84.6	9.42×10^{-3}	0.265	I

FIG. 2. Case CNTL: vertical cross section of the vertical velocity (in m s^{-1}; shaded) and potential temperature (solid lines) produced by a uniform, conditionally unstable flow over a two-dimensional mountain ridge with the mountain peak of 2 km, half-width of 30 km, and basic flow of 5 m s^{-1}. The unsaturated moist Froude number (F_w) is 0.262. The flow fields are shown at (a) 3 and (b) 7 h. The contour interval for potential temperature is 7 K. The cloud boundary is denoted by the thick dotted curve for total water content greater than 0.0005 g kg^{-1}.

namely, a growing mode and a propagating mode as classified by Lin et al. (1998) for convective cells embedded in a multicell storm. The growing mode (Fig. 4) may also be called a forced mode, which is produced mainly by the latent heating associated with the microphysical processes of the convective cells, while the propagating mode behaves like a free gravity wave. The propagating mode proposed by Lin et al. (1998) is similar to the trapped gravity mode (developed at a later

stage) in Yang and Houze (1995). The vertical velocity and diabatic heating are in phase with the growing mode, as also assumed in the linear theory developed in Yang and Houze (1995). In the present case, after $t =$ 7 h, six convective cells located at $x = -72, -69, -61, -56, -48$, and -38 km (Fig. 4a) may be classified as growing or forced modes. Note that the adiabatic warming associated with subsidence is much weaker than the warming produced by latent heating associated
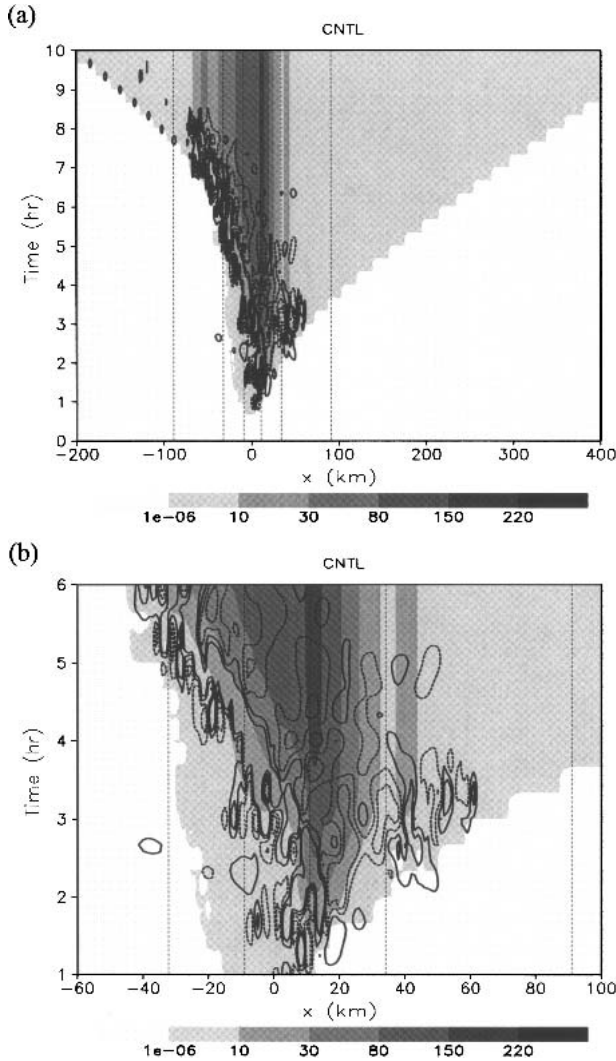
(a)

(b)

FIG. 3. Case CNTL: (a) Time evolution of the vertical velocity at 3.6-km height (contour lines are shown at -3, -1, 1, and 3 m s^{-1}) and accumulated rainfall and (b) an enlarged figure of (a) around $x = 0$ km. Rainfall greater than 0.1 mm is shaded. Dotted lines indicate elevation (200, 1000, and 1800 m) where the mountain peak is at $x = 0$ km.

with the convective updrafts. On the other hand, convective cells located at $(x, z) = (-7$ km, 9 km$)$ in Fig. 2a and at $(x, z) = (-38$ km, 8 km$)$ in Fig. 2b possess quite different characteristics from the convectively forced modes (e.g., Lin et al. 1998). Upon closer inspection, one can see that this convective cell has a phase difference between the vertical velocity and potential temperature perturbation. More specifically, the updraft is located 1/4 wavelength behind the maximum temperature perturbation. This relationship is explained by basic linear gravity wave theory (see Lin et al. 1998; Yang and Houze 1995).

In the lower layer near the surface (Fig. 4b), a deep cold pool extending approximately to $x = -70$ km is

produced by evaporative cooling associated with rainfall along the windward slope of the mountain. The cold pool develops into a density current, which propagates against the basic wind. The dynamics associated with the force balance between the cold pool and the uniform basic wind is controlled by the parameter, $U/(Qld)^{1/3}$, where Q is the buoyancy depletion or evaporative cooling rate (in K s^{-1}) and l and d are the horizontal scale and vertical depth of the cooling region (Thorpe et al. 1980). Apparently, the present case belongs to the subcritical flow regime with respect to the outflow (i.e., the cold pool); thus a density current can form and propagate upstream against the basic flow. In fact, by comparing the flow fields in Figs. 2a and 2b more carefully, one can see that in addition to the upstream propagation of the density current, there are upstream-propagating gravity waves generated by the convective system, such as the convective cell centered at $(x, z) = (-7$ km, 9 km$)$ in Fig. 2a and the one centered at $(x, z) = (-38$ km, 8 km$)$ in Fig. 2b. Dynamically, this flow belongs to a regime subcritical to both outflow and gravity waves (Raymond and Rotunno 1989; Lin et al. 1993) since both features are able to propagate upstream against the basic wind. Note that the propagation of internal gravity waves is controlled by the nondimensional parameter, $\pi U/Nd$ (Raymond and Rotunno 1989), where N is Brunt–Väisälä frequency and d the depth of the prescribed cooling layer. This type of flow is consistent with Fig. 14a in Lin et al. (1993).

Effects of F_w on the moist flow regimes and the regime transition may be investigated systematically by varying F_w, similar to that carried out in CL. The variation of F_w is performed by varying the basic wind velocities from 2.5 to 30 m s^{-1} (for CP4FX cases), which gives $F_w = 0.131$ to 1.572. Figure 5 shows the vertical velocity and potential temperature at 7 h for cases CP4F1, CP4F3, CP4F4, and CP4F6 and the corresponding time evolutions of the vertical velocity at 3.6-km height and accumulated rainfall. Case CP4F1 (Figs. 5a and 5e) is similar to the CNTL (CP4F2) case except with $F_w = 0.131$ ($U = 2.5$ m s^{-1}). As in the CNTL case, in addition to a slowly moving convective system at earlier times over the mountain peak, there is an upstream-propagating convective system after $t = 3$ h. Apparently, this flow belongs to regime I, as in the CNTL case. After $t = 7$ h, the system starts to weaken rapidly (Fig. 3a) and keeps propagating upstream. Figures 5b and 5f show the same fields as those in Figs. 5a and 5e, respectively, except for case CP4F3 ($F_w = 0.524$; $U = 10.0$ m s^{-1}). A long-lasting convective system remains on the lee side near the mountain peak during the simulation period, and the maximum rainfall is located on the lee slope in the region between $x = 50$ km and $x = 100$ km. Near the top of the windward slope there exists another mixed type of cloud system (transition between convective and stratiform) during the entire simulation period. Following Stein (2004), strati-
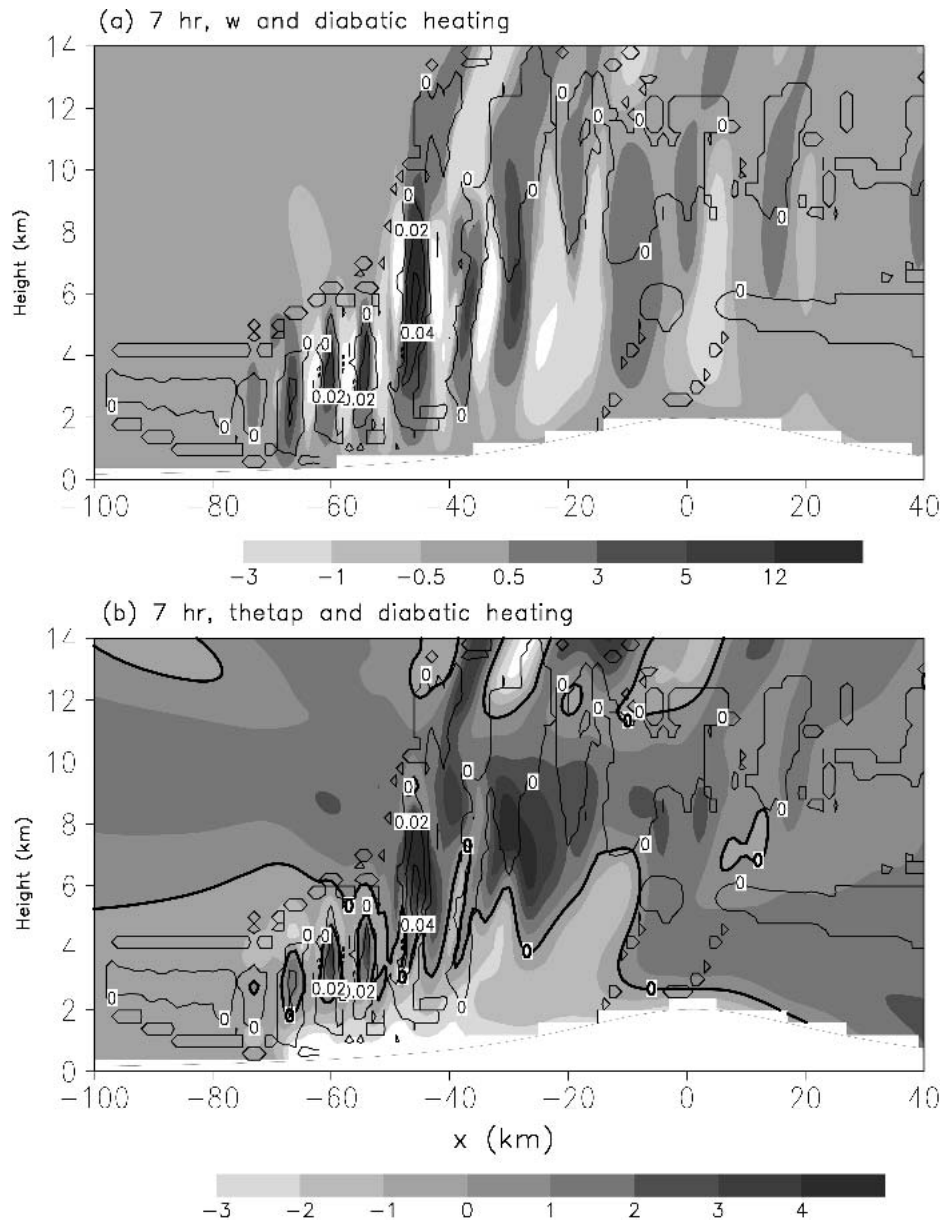
FIG. 4. (a) Vertical velocity (shaded) and diabatic heating (contour lines with 0.02 K s^{-1} intervals) and (b) potential temperature perturbation (shaded; K) and diabatic heating (contour lines with 0.02 K s^{-1} intervals) at 7 h. The heavy thick line in (b) is the 0 value of potential temperature perturbation.

form clouds are defined as clouds with depths less than 4 km. As depicted in the temporal sequence of accumulated rainfall (Fig. 6a), these two cloud systems are responsible for producing the rainfall over the mountain peak and along the lee slope. Based on CL's classification, this flow might be classified as regime II, that is, a long-lasting convective system located over the mountain peak. We therefore classify the flow of this case, whose convective system remains in the vicinity of the mountain peak, as regime II, but note that the convective system may stay at either the windward or lee slope.

Figures 5c and 5g show the same fields as those in Figs. 5a and 5e, respectively, except for case CP4F4 (F_w = 1.048; U = 15.0 m s^{-1}). The major difference between these two cases is that the convective system continuously propagates downstream. A severe downslope wind (e.g., Smith 1985) with a maximum wind greater than 40 m s^{-1} can be found over the lee slope (Fig. 7), which is much stronger than that in the CNTL case and which appears to help advect the convective system farther downstream. This strong downslope wind helps to produce a hydraulic jump and its accompanying strong convergence, crucial in generating the
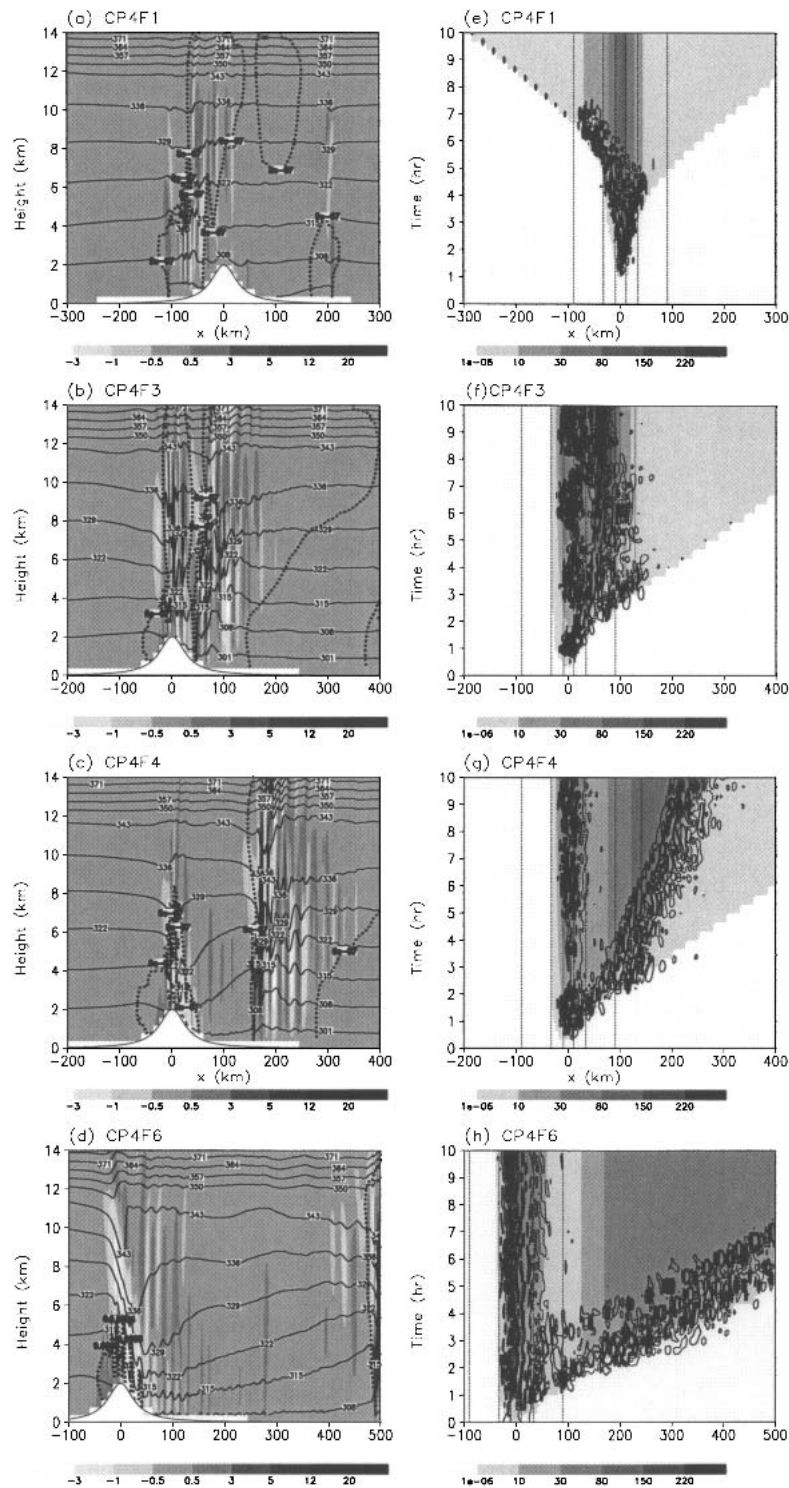
FIG. 5. The vertical velocity (in m s^{-1}; shaded) and potential temperature (K) at 7-h simulation for (a) CP4F1, (b) CP4F3, (c) CP4F4, and (d) CP4F6, and (e), (f), (g), and (h) the corresponding time evolutions of the vertical velocity at 3.6-km height (contour lines are shown at -3, -1, 1, and 3 m s^{-1}) and accumulated rainfall, respectively (see Table 1 for details). Rainfall greater than 0.1 mm is shaded. Dotted lines indicate elevation (200, 1000, and 1800 m) where the mountain peak is at $x = 0$ km. The cloud boundary is denoted by the thick dotted curve for total water content greater than 0.0005 g kg^{-1}.

FIG. 7. Vertical cross section of zonal flow (in m s^{-1}) with a basic flow of 20 m s^{-1} after a 7-h simulation. The unsaturated moist Froude number (F_w) is 0.786 (CP4F4). The contour interval for zonal flow is 10 m s^{-1}.

FIG. 6. Spatial distribution of total accumulated rainfall (mm) after 4-h (thin solid line), 6-h (thick solid line), 8-h (thin dashed line), and 10-h (thick dashed line) simulations for (a) CP4F3 and (b) CP4F4. The environmental thermodynamic sounding is the same as CNTL case.

downstream-propagating convective system along its front edge. From the temporal sequence of accumulated rainfall (Fig. 6b), one can clearly see that a long-lasting convective system, which is a mixed type of cloud system (transition between convective and stratiform), remains close to the top of the mountain during the simulation in addition to a convective system which propagates downstream. This flow belongs to regime III.

The setting of case CP4F6 (Figs. 5d and 5h) is similar to that of CP4F4 but with a larger unsaturated moist Froude number ($F_w = 1.572$; $U = 30$ m s^{-1}). The flow characteristics in this case are different from those in CP4F4 during the simulation period. In this case (CP4F6), the updraft over the mountain peak is tilted upstream, and only straiform-type clouds exist. However, in CP4F4 (regime III), the orographic cloud is a mixed type (transition between convective and stratiform), and the updraft is deeper and more erect (this can also be seen from the potential temperature field
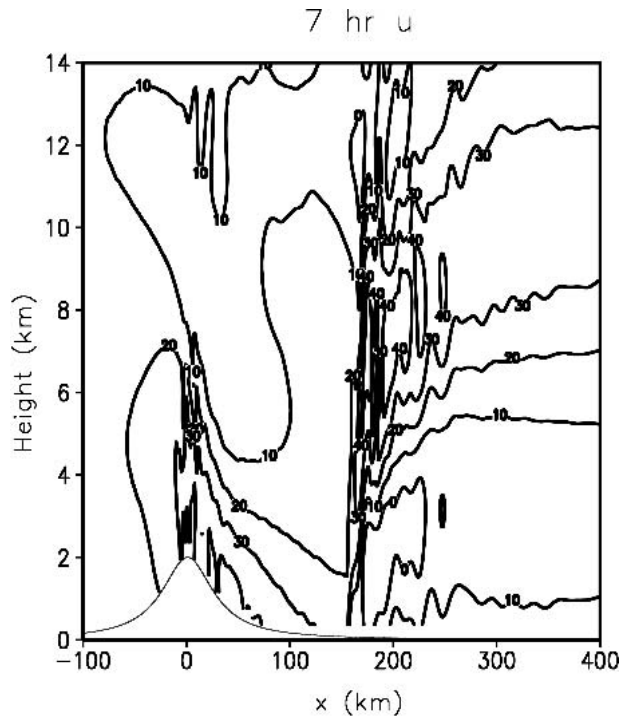
above the mountain peak). Therefore, CP4F6 is categorized as a new flow regime, that is, regime IV.

One may raise the following question: why is an orographic stratiform cloud, instead of a convective type (e.g., CP4F3), formed over the mountain in CP4F6? Whether convective or stratiform types of cloud are formed may be determined by the advection time and the cloud growth time. The advection time can be estimated by a/U, where a is the mountain half-width. The cloud growth time is controlled by the microphysical processes, which are rather complicated and difficult to estimate (e.g., Jiang and Smith 2003). Assuming the cloud growth time is 20 min (e.g., Stein 2004), the advection time for CP4F6 is about 16 min, which is barely enough for a deep (convective) cloud to develop. On the other hand, the advection time for CP4F3 is about 50 min, which is long enough for a convective cloud to develop. Another relevant time scale is the orographic perturbation growth time. The orographic perturbation growth time is related to the strength of the conditional instability. Assuming the mountain is high enough to lift the impinging conditionally unstable airstream to the LFC, then the orographic perturbation growth time is related to CAPE and may be estimated by cloud depth, and the averaged vertical velocity induced by the conditional instability. Along this line of thinking, we may roughly estimate the orographic perturbation growth time to be ($z_{LNB} - z_{LFC})/W_{ave}$, where W_{ave} may

be estimated by half the value of $W_{max} = \sqrt{2CAPE}$. A rough estimate gives the orographic perturbation growth time of about 4 min for both CP4F6 and CP4F3, which is apparently short enough for air parcels to penetrate to the tropopause but is too short compared with the cloud growing time for these two cases and is less relevant to the cloud development. Thus, in this situation, the cloud type (i.e., convective versus stratiform) will be determined by the advection time and the cloud growing time.

Based on Fig. 5, varying F_w tends to produce transition from regime I to II, III, and then to IV. One might be able to draw an analogy between the moist flow and the dry flow regimes by linking the current regime I to blocked dry flow with columnar disturbance, regimes II and III to breaking dry mountain wave, and regime IV to the quasi-linear dry flow. The downstream-propagating convective system in regime III is triggered by the convergence associated with the hydraulic jump; thus it is linked to the breaking dry mountain wave since the generation of a hydraulic jump over the lee slope is related to the wave breaking (e.g., see Smith 1985). Lin and Wang (1996) presented a series of figures showing the flow regime transition for dry flow over mountains, which may be used for comparison.

Figure 8 shows the spatial distribution of total accumulated rainfall after a 10-h simulation with CAPE = 3000 J kg^{-1} and different basic flow velocities. For all cases, there is an area of local maximum rainfall near the mountain peak, which is associated with the oro-

graphic lifting. The accumulated rainfall spreads (or the precipitating system propagates) upstream for cases CP4F1 and CNTL (CP4F2) but downstream for the other cases. The simulated convective system is able to consistently propagate farther downstream when the basic flow speed increases.

As found in CL and Chen and Lin (2004), the flow tends to shift to a higher number flow regime as F_w increases while using the thermodynamic sounding shown in Fig. 1. In addition, we have identified one new flow regime (regime IV). The definition of regime I as proposed by CL has also been modified to include an early, slowly moving convective system in the vicinity of the mountain peak, in addition to the upstream-propagating convective system, which possibly weakens before the end of the numerical simulation. Regime II, as proposed by CL, is modified to have a long-lasting convective system remaining in the vicinity of the mountain peak, but the convective system may stay at either the windward or lee slope.

b. Effects of CAPE

The speed of the density current, which is proportional to the strength of the cold pool, can help determine the propagation speed of the convective system. The strength of the evaporative cooling, which is one of the major factors in determining the strength of the cold pool, is in turn closely related to the magnitude of CAPE in a conditionally unstable flow. Therefore, the propagation of a convective system might be strongly
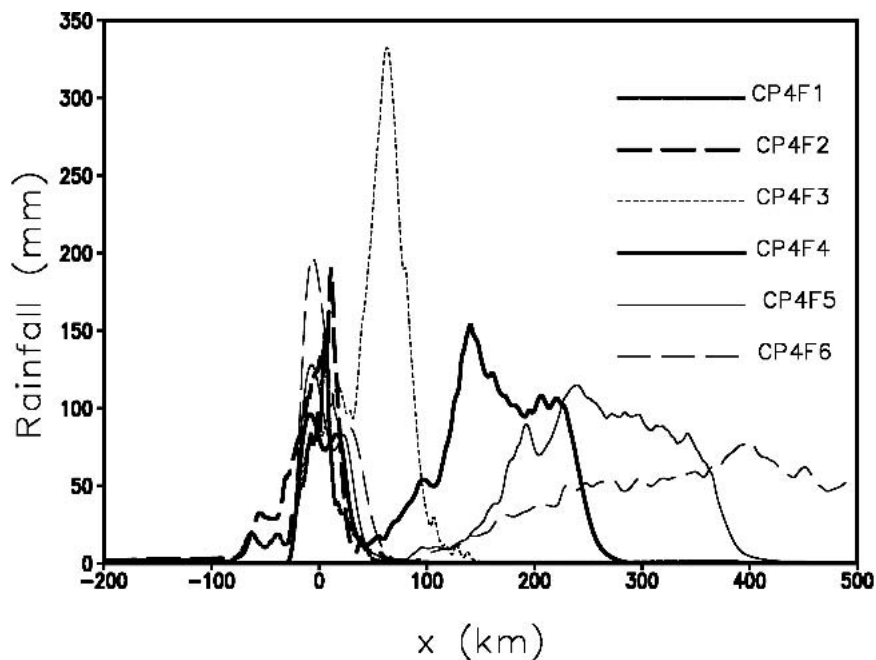

FIG. 8. Total accumulated rainfall (mm) after 10-h simulation for CP4F1 (thick dotted line), CNTL (CP4F2; thick long-dashed line), CP4F3 (thin dotted line), CP4F4 (thick solid line), CP4F5 (thin solid line), and CP4F6 (thin long-dashed line). The environmental thermodynamic sounding for all cases is the same as the CNTL case, and the CAPE is about 3000 J kg^{-1}.

correlated to the magnitude of CAPE in the atmosphere. In addition, CAPE is correlated to the saturated moist Froude number by N_m, which might be an important variable in the second nondimensional control parameter (still unknown at the time of research), as it is derived here. The definition of CAPE in Eq. (1) may also be written as (e.g., see Emanuel 1994)

$$\text{CAPE} = \int_{z_1}^{z_2} B \, dz, \tag{5}$$

where B is the buoyancy and z_1 and z_2 are the LFC and the LNB, respectively. In cloudy air, the buoyancy is related to the saturated Brunt–Väisälä frequency (N_m), which is related to B by $N_m^2 = -\partial B/\partial z$. Thus, CAPE is related to the saturated Brunt–Väisälä frequency by

$$\text{CAPE} = \int_{z_1}^{z_2} \left(-\int N_m^2 \, dz \right) dz \approx -\frac{1}{2} \overline{N}_m^2 (z_2^2 - z_1^2), \tag{6}$$

where $\overline{N}_m$ is the column-averaged saturated Brunt–Väisälä frequency. Note that $N_m^2 < 0$ for a statically unstable, moist air. Thus, roughly speaking, CAPE is directly proportional to $|N_m^2|$. The vertical acceleration of cloudy air is related to the saturated Brunt–Väisälä frequency by (e.g., Emanuel 1994)

$$\frac{d^2 \delta z}{dt^2} + N_m^2 \delta z = 0, \tag{7}$$

where the first term is the vertical acceleration of a moist air parcel and δz is the vertical displacement of the air parcel from its undisturbed level. Therefore, the larger the CAPE, the stronger the vertical acceleration and the stronger the convective system. However, it is worth mentioning that the strength of convective systems can also be modified by the orographic forcing.

Based on a limited number of preliminary numerical experiments, it is found that, when the CAPE decreases, the moist upstream flow tends to shift to a higher Froude-number regime for both two- (Chu and Lin 1998) and three-dimensional flow (Chen and Lin 2004). To investigate the effects of CAPE on the generation and propagation of orographically generated precipitation systems more completely, we make six idealized simulations (CP0F2, CP1F2, CP2F2, CP3F2, CP4F2, and CP5F2; see Table 1) with varying amounts of CAPE by changing the model atmospheric temperature profile above 2.0 km. The soundings for these cases are shown in Fig. 9. The CAPE values for cases CP0F2, CP1F2, CP2F2, CP3F2, CP4F2 (CNTL), and CP5F2 are 487, 1372, 1895, 2438, 3000, and 3578 J kg^{-1}, respectively (Table 1). Figure 10 shows the vertical cross sections of vertical velocity and potential temperature for these cases after $t = 7$ h. Note that the convective system is located farther upstream when the CAPE increases. For cases CP1F2 and CP2F2, the simulated
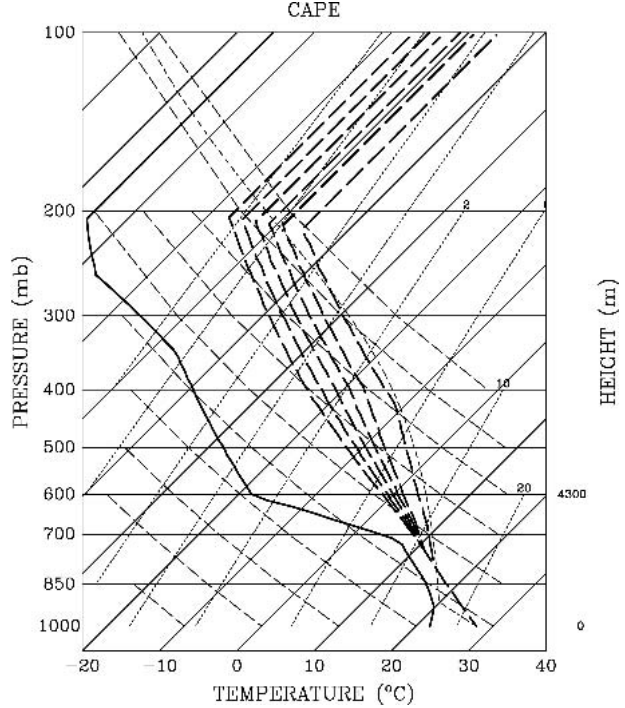

FIG. 9. Long-dashed lines (temperature profiles) from right to left are soundings for the CP0F1, CP1F2, CP2F2, CP3F2, CNTL (CP4F2), and CP5F2 cases, respectively. The CAPE values for them are 487, 1372, 1895, 2438, 3000, and 3578 J kg^{-1}, respectively. The basic wind speed is $U = 5$ m s^{-1}.

convective systems remain on the lee side near the mountain peak, a situation similar to case CP4F3. Therefore, both CP1F2 and CP2F2 may be classified as regime II. Recall that case CP4F3 has a larger F_w (basic flow) and a larger CAPE. For case CP3F2, a long-lasting convective system develops near the top of the mountain. Therefore, it is classified as regime II, in which a long-lasting convective system remains in the vicinity of the mountain peak on either the windward side or lee slope side. Note that the convective system eventually dissipates at the end of simulation. Figure 10d shows simulation result from CP5F2, which is very similar to that in CNTL case. Therefore, we classify it as flow regime I.

Figure 11 shows the spatial distributions of total accumulated rainfall produced by cases CP1F2–CP5F2 after a 10-h simulation. The location of the maximum accumulated rainfall shifts upstream, and the density current intensifies (Fig. 10d) as the flow regime shifts to a smaller number flow regime when the environmental CAPE increases (Table 1).

c. Regime diagram with control parameters F_w and CAPE

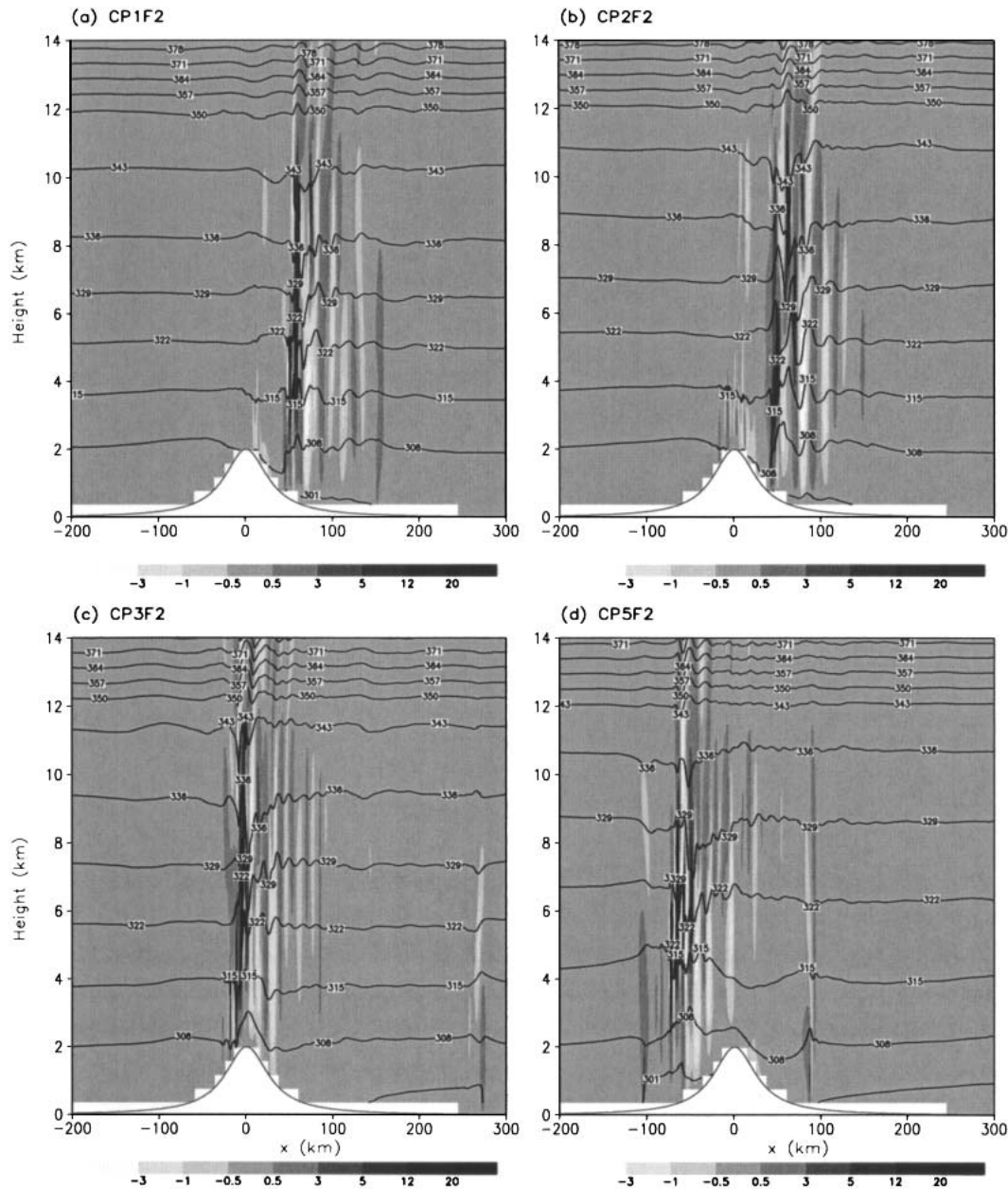From the simulation results obtained above, it becomes clear that both the unsaturated moist Froude

FIG. 10. Vertical cross section of the vertical velocity (in m s^{-1}; shaded) and potential temperature (solid lines with a contour interval of 7 K) for (a) CP1F2, (b) CP2F2, (c) CP3F2, and (d) CP5F2 after 7-h simulation. The basic wind speed is 5 m s^{-1}.

number and CAPE may serve as control parameters for the classification of flow regimes. However, two important results may be questioned and they are related dynamically: 1) The flow tends to shift to a higher number flow regime when the unsaturated moist Froude number increases for a given thermodynamic sounding, and 2) the flow regime shifts to a lower number flow regime when the CAPE increases. To address these issues, we conduct a series of experiments (36 members in total) and vary two control parameters, F_w and

CAPE, to help determine the two-dimensional flow regime diagram. In these experiments, F_w is varied by changing the basic wind speed from 2.5 to 30 m s^{-1} (CPXF1–CPXF6). The CAPE varies from 487 to 3578 J kg^{-1} for CP0FX –CP5FX.

Based on F_w and CAPE, we have constructed a moist flow regime diagram, presented in Fig. 12, analogous to the dry flow regime proposed in Smith (1989). From the figure, we can see that with a relatively large and fixed CAPE (e.g., greater than 1800 J kg^{-1} in this study), the
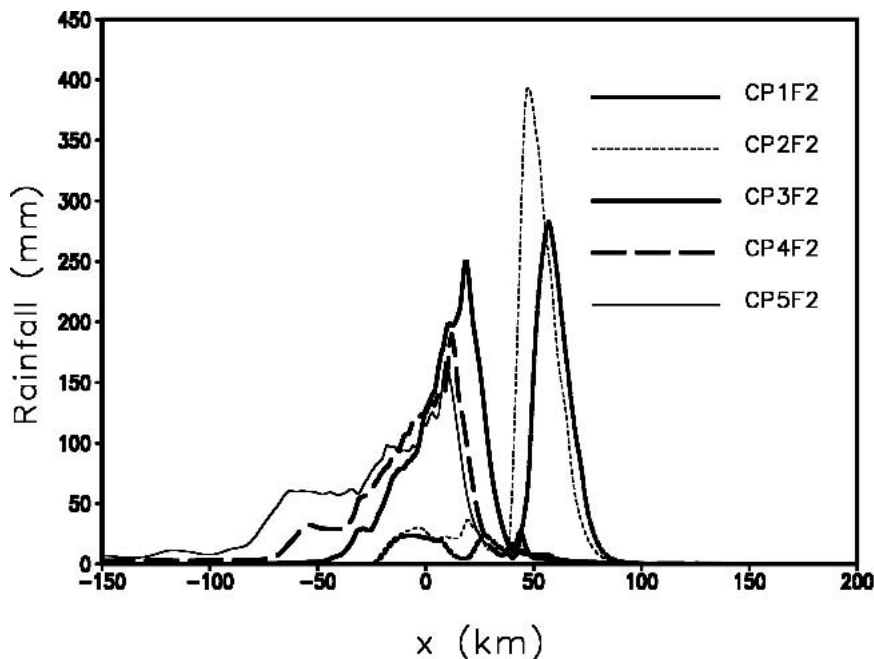
FIG. 11. Total accumulated rainfall (mm) after a 10-h simulation for CP1F2 (thick dotted line), CP2F2 (thin dotted line), CP3F2 (thick solid line), CNTL (CP4F2; long-dashed line), and CP5F2 (thin solid line) with a basic flow of 5 m s^{-1}.

flow is shifted toward a larger number flow regime in a successive sequence as the F_w increases. However, when the CAPE is small (say, less than 400 J kg^{-1}), there exists a possible bifurcation point, which sepa-
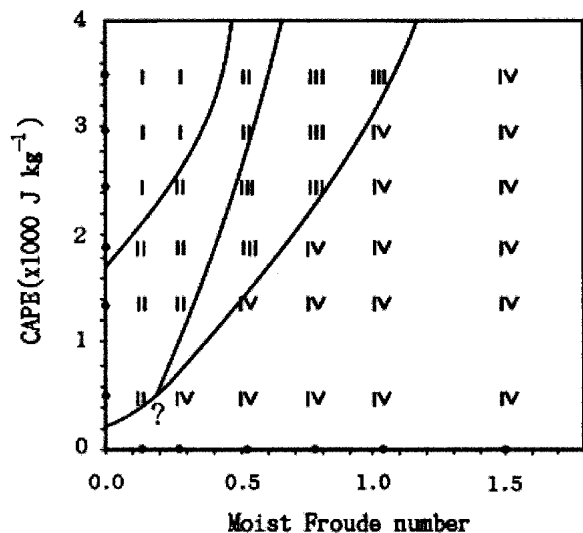

FIG. 12. Flow regimes on the control parameters F_w, and CAPE. The CAPE increases from 487 (CP0), 1372 (CP1), 1895 (CP2), 2438 (CP3), 3000 (CP4), to 3578 (CP5) J kg^{-1}. The last five thermodynamic profiles are those used for CP1F2, CP2F2, CP3F2, CP4F2 (CNTL), and CP5F2 in section 3b. The sounding for CP0 is obtained the same way as other CPX cases, whose temperature profiles are modified from that in Fig. 1. The basic wind increases from 2.5 to 30 m s^{-1}, which gives F_w = 0.131 to 1.572.

rates regimes II, III, and IV of the moist flow regime when F_w is small (e.g., 0.16). Incidentally, based on the horizontal mountain scale aspect ratio and nondimensional mountain height, Smith (1989) found a bifurcation point separating four dry flow regimes: mountain wave, flow splitting, wave breaking, and flow splitting and wave breaking. Ideally, the flow characteristics for cases with different basic wind speeds should be compared at the same nondimensional time, especially for steady-state or quasi-steady-state flow. However, our interest here is on the transient features of the convective systems. Thus, the classification for small F_w cases (e.g., CPXF1 cases) are based on 10-h simulated results. Comparison of Figs. 8 (larger CAPE) and 13a (smaller CAPE) shows that two different modes of precipitation systems, the orographically forced *long-lasting* precipitation system in the vicinity of the mountain and *the lee-side propagating* precipitation system, exist in both cases but behave very differently. When the CAPE is large, the difference in the rainfall amount produced by the long-lasting precipitation system over the mountain for different F_w (basic wind speeds) is relatively small, that is, it is less sensitive to F_w (basic wind speed; Fig. 8). On the other hand, with a small CAPE, the rainfall amount associated with the long-lasting precipitation system around the mountain is proportional to F_w (basic wind speed; Fig. 13a).

Physically and dynamically, the role of F_w and CAPE may be interpreted using the ingredient argument proposed by Lin et al. (2001a), which is similar to that in Doswell et al. (1996), and the orographic rain forecast-
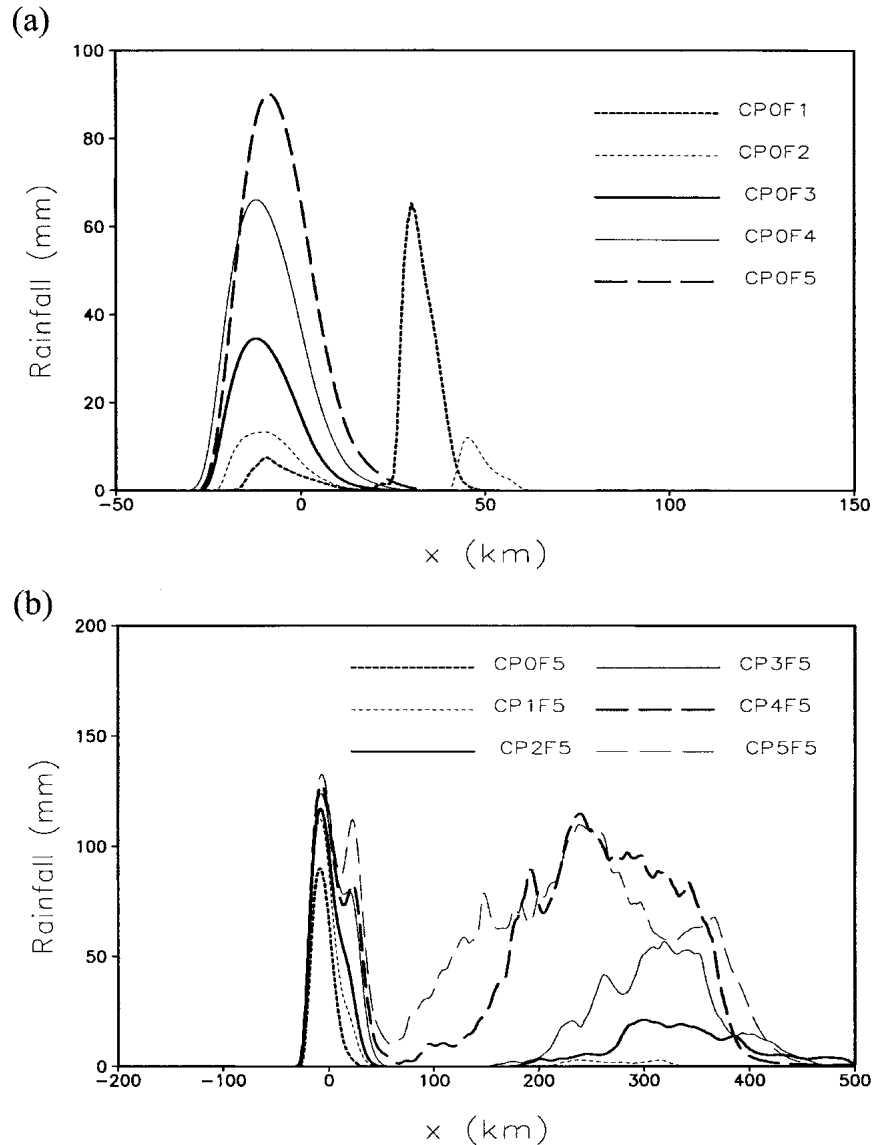
FIG. 13. Total accumulated rainfall (mm) after 10-h simulation (a) for CP0F1 (thick dotted line), CP0F2 (thin dotted line), CP0F3 (thick solid line), CP0F4 (thin solid line), and CP0F5 (long-dashed line) with CAPE $= 487$ J kg^{-1}, and (b) for CP0F5 (thick dotted line), CP1F5 (thin dotted line), CP2F5 (thick solid line), CP3F5 (thin solid line), CP4F5 (thick long-dashed line), and CP5F5 (thin long-dashed line) with a basic wind speed of 20 m s^{-1}.

ing models of Alpert (1986) and Smith (2003). The total precipitation (P) associated with an orographic precipitating system may be estimated as (see, e.g., Lin et al. 2001a)

$$P = (\rho/\rho_w)\, E(w_{\mathrm{oro}} + w_{\mathrm{env}})qD, \qquad (8)$$

where ρ is the low-level air density, ρ_w the liquid water density, E the precipitation efficiency, w_{oro} the upward motion induced by the orography, w_{env} the upward motion induced by the environment (such as conditional instability, convective instability, etc.), q the low-level mixing ratio of water vapor, and D the duration of the

precipitating system. Roughly, w_{oro} may be estimated by $U\partial h/\partial x$ for flow over a two-dimensional mountain ridge. For a conditionally unstable airstream, w_{env} may be estimated by the idealized equivalent vertical velocity, W_{max}, which is roughly equal to $\sqrt{2\mathrm{CAPE}}$. Note that the relationship between w_{oro} and w_{env} may not necessarily be linear since the convective systems induced by these two types of forcing are highly nonlinear and may interact with each other. Additionally, these two values should not be compared quantitatively but qualitatively since w_{oro} ($=U\partial h/\partial x$) is just an estimation of the vertical velocity at the surface, while

w_{env} ($=\sqrt{2CAPE}$) is an estimation of the maximum vertical velocity inside the convective cell for a conditionally unstable flow. It is worth mentioning that the vertical moisture profile in the model atmosphere is kept the same for all cases studied here (only the basic wind speed or temperature profile is changed).

Consider the situation with relatively large CAPE (e.g., Figure 8). In this case, w_{env} will dominate the vertical motion, but a modest w_{oro} may be able to induce an orographic convective system associated with the long-lasting mode in the vicinity of the mountain, as long as the LFC is reached. Hence, the rainfall amount will be less sensitive to the magnitude of w_{oro}, or rather the basic wind speed because the slope steepness ($\partial h/\partial x$) is fixed in this case. On the other hand, for the case with small CAPE (e.g., Fig. 13a), the vertical velocity induced by the conditional instability might be relatively small, and the orographic rainfall amount will be more sensitive to the basic wind since $w_{oro} = U\partial h/\partial x$. Thus, orographic rainfall amount is roughly proportional to the basic wind speed, or F_w, if the mountain slope remains unchanged. Implicitly, this indicates that conditional instability does not play an important role in producing orographic rainfall when the basic wind speed is large (Fig. 13b). Therefore, with small CAPE and large basic wind speed, the *long-lasting orographic precipitation system over the mountain belongs to the stratiform type, instead of the convective type,* due to the classical stable accent mechanism (e.g., see reviews by Smith 1979, Houze 1993, and Chu and Lin 2000). This is evidenced by the vertical velocity, potential temperature, and shallow cloud fields for the case with $U = 20$ m s^{-1} and CAPE = 1372 J kg^{-1} (see Fig. 14d). As mentioned earlier, the stratiform cloud is defined as having a cloud depth less than 4 km. Under this condition, since the convective precipitation system is dominated by the orographically induced vertical motion, it should reflect the structure of the mountain shape. Here the vertical motion field reveals a hydrostatic mountain wave (Fig. 14d). The-lee-side propagating convective or cloud system is very weak, and therefore this flow regime may be referred to as a long-lasting *orographic stratiform precipitation system over the mountain* and possibly a *downstream-propagating cloud system*. Note that this is a new flow regime (regime IV), which was not discussed in CL and Chen and Lin (2004).

From a fundamental physics point of view, one might be curious to know why a deep, orographic convective system cannot develop when the basic wind is strong and the environmental CAPE is small. For the CP1F2 sounding (Fig. 9), the LFC is located at about 820 hPa, which is about 1.8 km. With a 2-km-high mountain, one would anticipate that the mountain is high enough to lift most of the low-level air parcels to their LFCs and release the instability even though the CAPE is not very large. Indeed, this is true. If one inspects case CP1F1, $F_w = 0.131$ and CAPE = 1372 J kg^{-1} (Fig. 14b), a deep convective system can be triggered in the vicin-

ity of the mountain under a small CAPE condition. This may be explained as follows: for weak basic flow, such as in CP1F1 (2.5 m s^{-1}), the advection time for airflow to cross the mountain is long enough for a deep cloud to develop over the mountain (Jiang and Smith 2003) due to the small CAPE (1372 J kg^{-1}). The kinetic energy (KE) associated with the cold pool produced by evaporative cooling is comparable to the KE associated with the weak basic flow. Thus, a quasi-steady, critical state is reached and convection is able to develop. In other words, the flow is *critical* to the *cold-air outflow*. On the other hand, for stronger wind and smaller CAPE (Fig. 14d), the deep convective cloud has insufficient time to grow over the mountain (small advection time). Since the KE associated with the cold air outflow is much smaller than the KE associated with the basic wind, the precipitating system will be advected downstream by the basic wind and no strong deep clouds can exist over the mountain area. In other words, the flow is *supercritical* to the *cold-air outflow*.

A similar situation also occurs with variation of CAPE when F_w (basic flow speed) is kept constant. When the basic flow is weak (say, e.g., less than or equal to 5 m s^{-1} in this study), the flow is shifted to a smaller number flow regime (i.e., the system moves upstream; see Fig. 11) as the CAPE increases (Fig. 12). This can be interpreted as follows: a stronger system on the lee side of the mountain can develop when an airstream has a larger CAPE and a weak basic flow (long advection time) and, therefore, the cold pool produced by the system is relatively stronger. Thus, under this situation the convective system on the lee slope is able to propagate upstream against the basic flow and shifts the flow to a smaller number flow regime. This, in a way, is analogous to the decrease in F_w (incoming wind speed) for a fixed CAPE.

The above discussions may be depicted by using the vertical velocity, potential temperature, and cloud fields in Fig. 14 and the temporal evolution of accumulated rainfall and the vertical velocity at 3.6-km height in Fig. 15 from four cases (CP1F1, CP5F1, CP1F5, and CP5F5). Based on Figs. 14a and 15a, the flow may be classified as regime I, which is characterized as a flow with an upstream-propagating convective system and a transient convective system existing in the vicinity of the mountain, which may potentially weaken at later times. Using Figs. 14b and 15b, the flow is classified as regime II.

From Figs. 14c and 15c, the flow is classified as regime III, which was characterized by a long-lasting orographic precipitation system near the mountain peak and a downstream-propagating convective system (CL). A closer inspection reveals that the long-lasting orographic precipitation system is a *mixed stratiform and convective precipitation system* (Fig. 14c). Note that, if the basic wind is weaker, then the long-lasting orographic precipitation system may be a convective type (e.g., Figs. 11 and 12 of CL) instead of a mixed
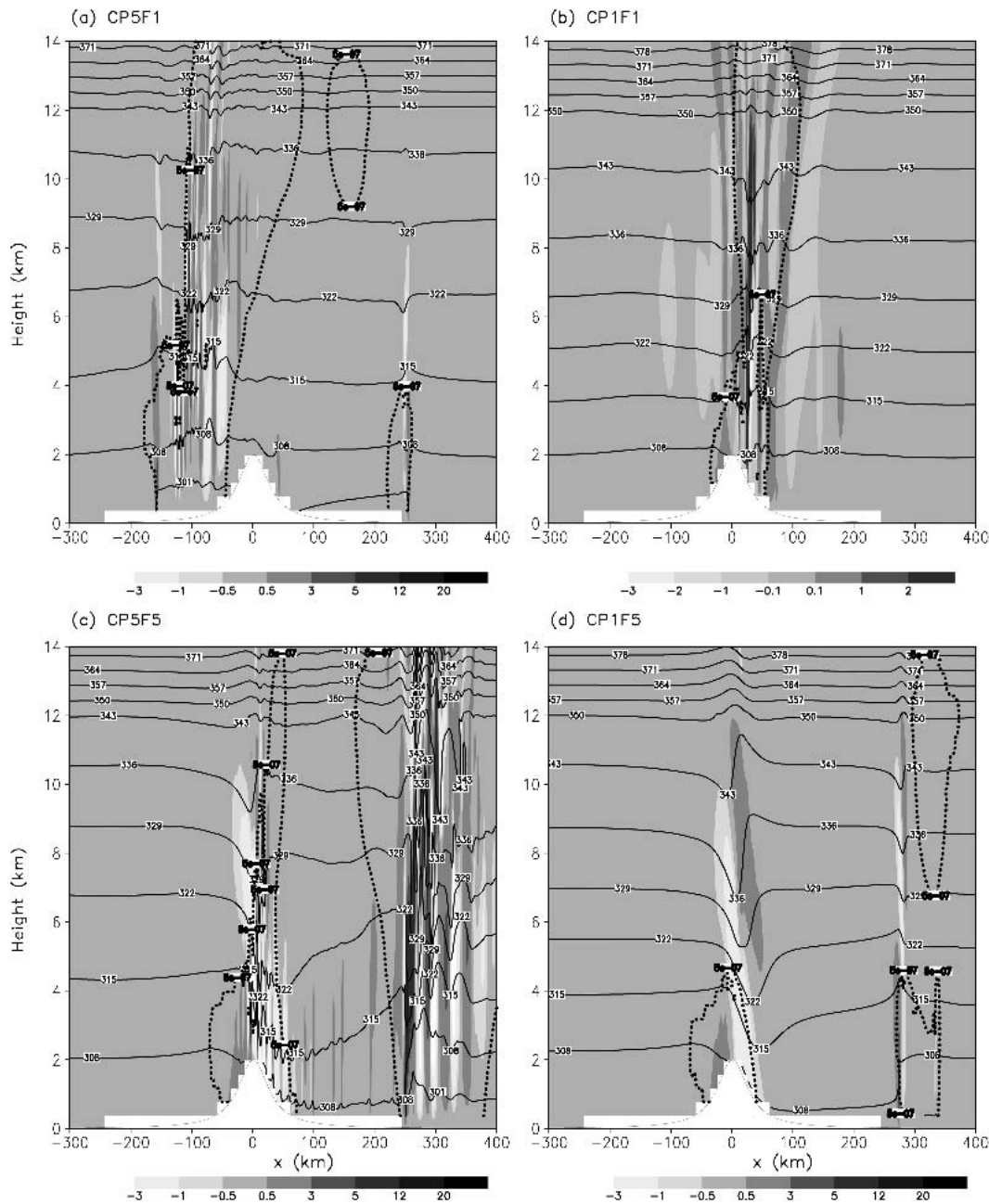
FIG. 14. Vertical velocity and potential temperature fields for (F_w, CAPE) = (a) (0.131, 3578 J kg^{-1}); (b) (0.131, 1372 J kg^{-1}); (c) (1.048, 3578 J kg^{-1}), and (d) (1.048, 1372 J kg^{-1}) after 7-h simulations. The cloud boundary is denoted by the thick dotted curve for total water content greater than 0.0005 g kg^{-1}.

type. In addition, due to the strong wind, an upward-propagating hydrostatic wave is produced, which can be seen clearly in the isentropes (Fig. 14c). From Fig. 15c, one can clearly see that the orographic precipitation system redevelops by $t = 4$ h, after the first convective system is advected downstream by the strong basic wind.

The flow shown in Figs. 14d and 15d was not identified in CL and Chen and Lin (2004); thus it is a new

flow regime as discussed above. This flow regime may be classified as regime IV and is characterized by a long-lasting orographic stratiform precipitation system and possibly a downstream-propagating cloud system. An upward-propagating hydrostatic mountain wave is produced by the strong basic flow. It is noted that a new downstream-propagating system is triggered at about 120 km (Fig. 15d) after 1.5-h simulation and starts generating light rainfall at 170 km after 2.5-h
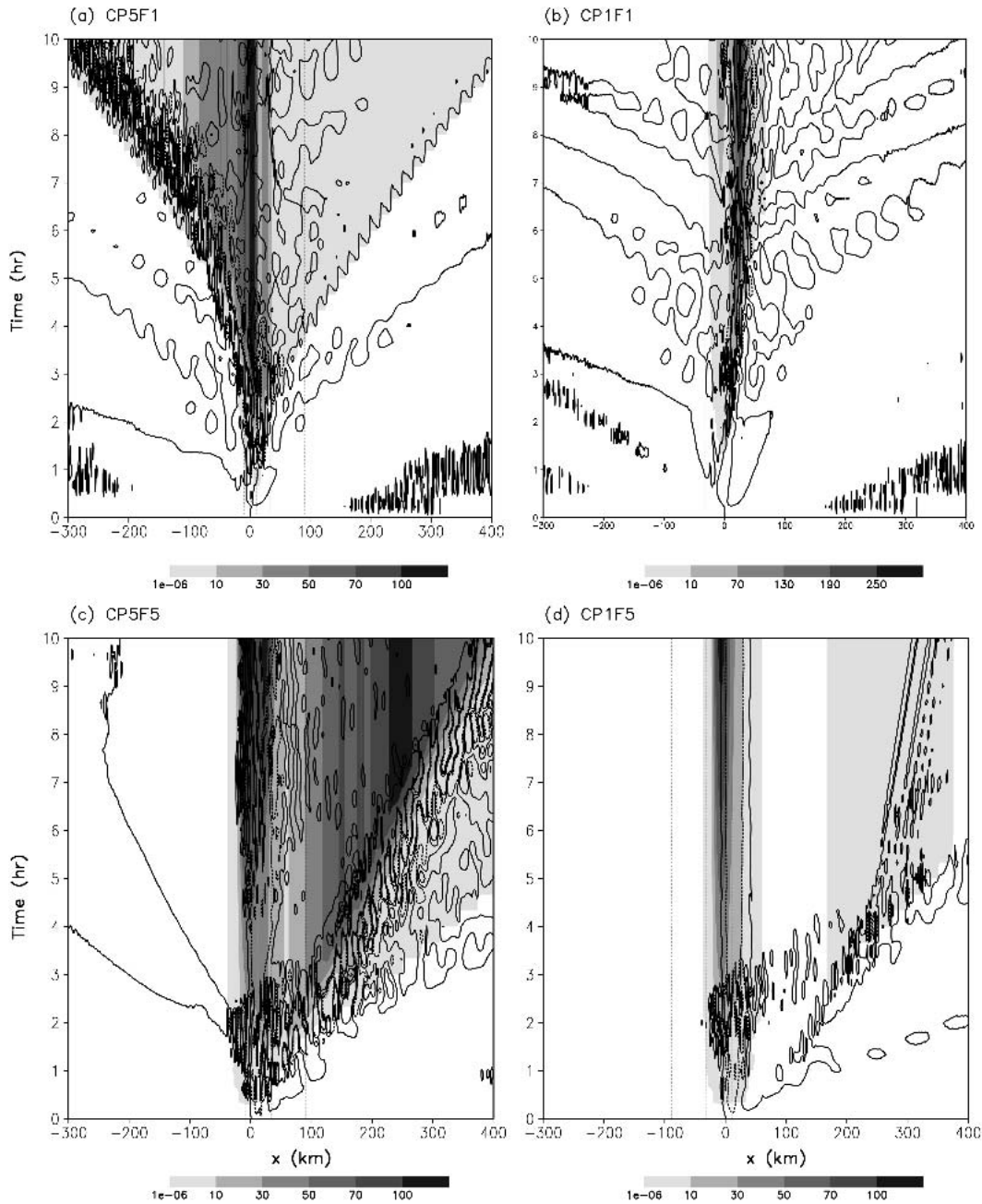
FIG. 15. Time evolution of the vertical velocity at 3.6-km height (contour lines are shown at -3, -1, 1, and 3 m s^{-1}) and accumulated rainfall for cases shown in Fig. 14. Rainfall greater than 0.1 mm is shaded. Dotted lines indicate elevation (200, 1000, and 1800 m), where the mountain peak is at $x = 0$ km.

simulation. This is why there is no rainfall between 70 and 180 km.

4. Concluding remarks

Based on idealized simulations of conditionally unstable flow passing over a two-dimensional mountain ridge, we found four moist flow regimes, which may be characterized as (Fig. 16) 1) regime I: flow with an upstream-propagating convective system and a transient convective system existing in the vicinity of the mountain at an earlier time; 2) regime II: flow with a long-lasting orographic convective system over the mountain peak, upslope or downslope; 3) regime III: flow with a long-lasting orographic convective or mixed convective and stratiform precipitation system over the mountain
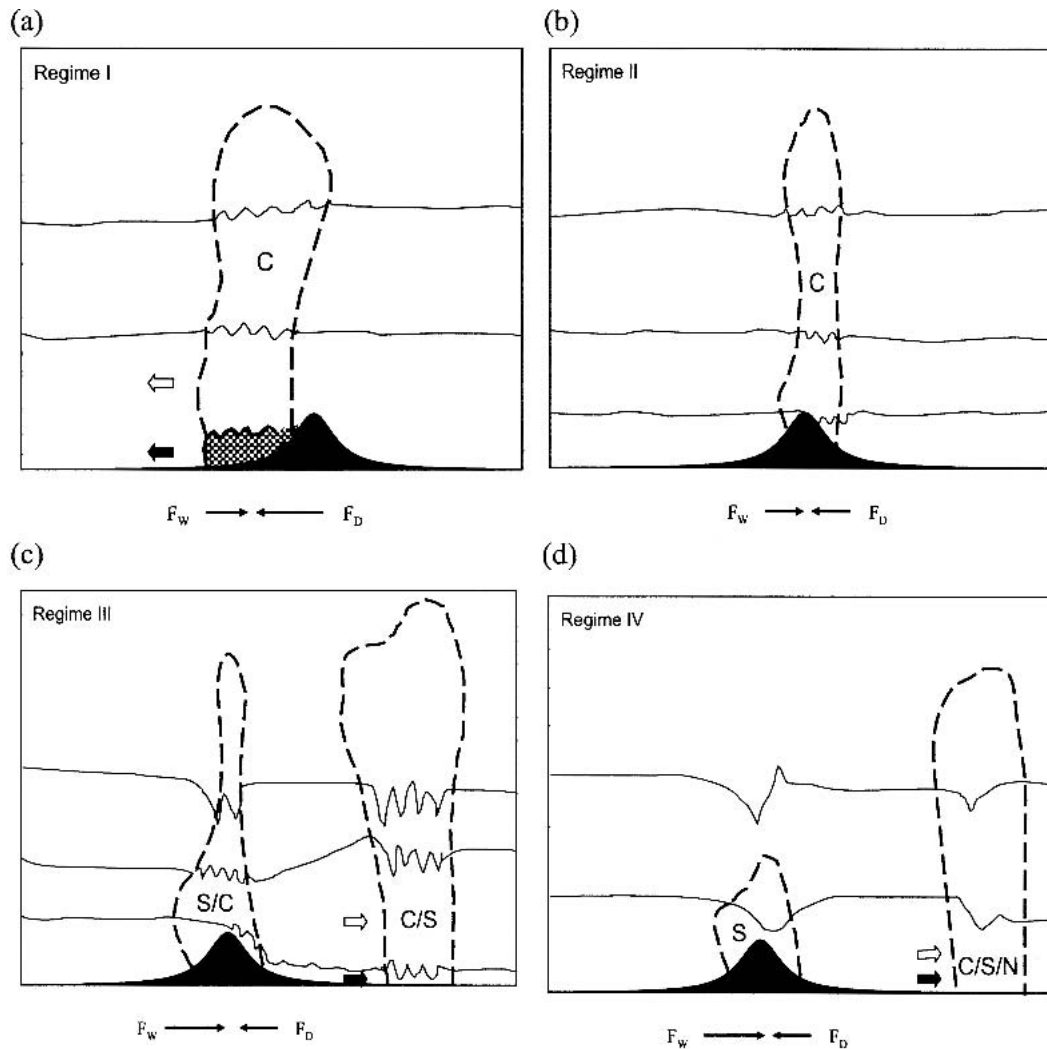
FIG. 16. Schematic of the flow regimes I–IV found in this study. 1) regime I: flow with upstream-propagating convective system and a transient convective system existing in the vicinity of the mountain at earlier time; 2) regime II: long-lasting orographic convective system over the mountain peak; 3) regime III: downstream-propagating convective system and long-lasting orographic convective or mixed convective and stratiform precipitation system; and 4) regime IV: a long-lasting orographic stratiform precipitation system over the mountain peak and possibly a downstream-propagating cloud system. Here, F_D is assumed to be a proxy of CAPE. Symbols C, S, and N denote convective, stratiform, and no cloud types, respectively. Outline (filled) arrow denotes the propagation direction of the precipitation system (cold-air outflow).

peak and a downstream-propagating convective system; and 4) regime IV: flow with a long-lasting orographic stratiform precipitation system over the mountain and possibly a downstream-propagating cloud system. Based on idealized simulations with variations in F_w and CAPE, a regime diagram is constructed. The first three flow regimes are the same as those found in CL and Chen and Lin (2004), but with modifications. Regime I proposed by CL has been modified to include a convective system in the vicinity of the mountain peak at an earlier time in addition to the upstream-propagating convective system, which may possibly weaken at later times. In regime II, the long-lasting

convective system may exist over the mountain peak, upslope, or lee slope instead of just over the mountain peak, as proposed by CL. For regime III, we found that the long-lasting orographic precipitation system over the mountain peak may become a mixed convective and stratiform precipitation system instead of just convective precipitation system proposed in CL. Note that the variation of F_w is carried out by varying U only. The fourth flow regime is new and was not discussed in CL and Chen and Lin (2004). The long-lasting orographic stratiform precipitation system in regime IV is explained by comparing the small advection time with cloud growing time; in addition, the kinetic energy of

the basic flow is much larger than that associated with the cold outflow produced by evaporative cooling; thus the precipitating system is advected downstream and a strong, deep convective system cannot develop over the upslope.

When the F_w (or basic wind speed) increases and the CAPE is fixed, the flow tends to shift to a higher number of the flow regime. Conversely, when the CAPE increases and the F_w (i.e., basic wind speed in this study) is fixed, the flow shifts to a lower regime. When the CAPE is large, the orographic rainfall amounts with different basic wind speeds are comparable (i.e., not sensitive to the basic wind speed) but the precipitation types can be different (i.e., convective versus stratiform). However, when the CAPE is small, the orographic rainfall amount is strongly dependent on the strength of the basic wind speed—the stronger the wind, the larger the amount of rainfall. The formation and propagation of different flow regimes may be interpreted by the competition between the forcing associated with the basic flow (F_w) and the forcing associated with the cold outflow or the density current (F_D), as shown in Fig. 16. The forcing associated with the cold outflow, F_D, is related to the CAPE. A more precise relationship between F_D and CAPE needs to be explored. The propagation and cloud types (convective, stratiform, or a mixed convective and stratiform) of the precipitation systems are determined by the time scaling (i.e., advection time and cloud growing time) and relative strength of the basic wind and the cold outflow, which may be represented by CAPE for a conditionally unstable flow.

In addition to F_w and CAPE, additional parameters may come into play to influence the moist flow regimes for a conditionally unstable flow over a mesoscale mountain. For example, the mountain height and width aspect ratio may serve as an important control parameter. To make a more complete moist flow regime diagram, a more complete coverage of the control parameters, which includes h/a, should be carried out. We will leave this for future studies. The readers are also reminded that our moist regime diagram is constructed based on reasonably long time simulated results, but not necessarily for steady or quasi-steady solutions. Longer time simulations, such as 20 h, for small F_w cases (e.g., CPXF1 cases) are also tested and the flow behavior is very similar to those for 10-h simulations (as presented) except for the CP5F1 case ($F_w = 0.131$ and CAPE $= 3578$ J kg^{-1}). In case CP5F1, a convective system redevelops near the peak of the mountain after a 13-h simulation and stays there until the end of the simulation. Thus, the moist flow regimes proposed in this study are based on transient, instead of quasi-steady state, numerical solutions. We have also tested the sensitivity of the moist flow to the initial orography setup by activating the microphysics processes after 10 h for some cases (CP2F1, CP0F2, and CP4F3). There exist some differences between these cases (20-h simu-

lations) and their counterpart experiments (e.g., cloud strength and cloud lifetime) that activate microphysics at $t = 0$ h. However, since we are interested in the transient moist flow regimes, our regime classifications for these new cases are still valid. Physically, this may be equivalent to a sudden increase of the environmental wind, such as the passage of a trough over the Alps in fall.

REFERENCES

Alpert, P., 1986: Mesoscale indexing of the distribution of orographic precipitation over high mountains. *J. Climate Appl. Meteor.,* **25,** 532–545.

Binder, P., and C. Schär, Eds., 1996: MAP design proposal. MeteoSwiss, 75 pp. [Available from the MAP Programme Office, MeteoSwiss, CH-8044, Zurich, Switzerland.]

Bougeault, P., and Coauthors, 2001: The MAP special observing period. *Bull. Amer. Meteor. Soc.,* **82,** 433–462.

Chen, S.-H., and J. Dudhia, 2000: Annual report: WRF physics. Air Force Weather Agency, 38 pp. [Available online at http://wrf-model.org.]

——, and W.-Y. Sun, 2002: A one-dimensional time-dependent cloud model. *J. Meteor. Soc. Japan,* **80,** 99–118.

——, and Y.-L. Lin, 2004: Orographic effects on a conditionally unstable flow over an idealized three-dimensional mesoscale mountain. *Meteor. Atmos. Phys.,* in press.

Chu, C.-M., and Y.-L. Lin, 1998: Effects of orography on the generation and propagation of mesoscale convective systems. Preprints, *Eighth Conf. on Mountain Meteorology,* Flagstaff, AZ, Amer. Meteor. Soc., 302–309.

——, and ——, 2000: Effects of orography on the generation and propagation of mesoscale convective systems in a two-dimensional conditionally unstable flow. *J. Atmos. Sci.,* **57,** 3817–3837.

Doswell, C. A., III, H. Brooks, and R. Maddox, 1996: Flash flood forecasting: An ingredient-based methodology. *Wea. Forecasting,* **11,** 560–581.

Emanuel, K. A., 1994: *Atmospheric Convection.* Oxford University Press, 580 pp.

Houze, R. A., Jr., 1993: *Cloud Dynamics.* Academic Press, 573 pp.

Jiang, Q., and R. B. Smith, 2003: Cloud timescales and orographic precipitation. *J. Atmos. Sci.,* **60,** 1543–1559.

Lin, Y.-L., and T. A. Wang, 1996: Flow regimes and transient dynamics of two-dimensional stratified flow over an isolated mountain ridge. *J. Atmos. Sci.,* **53,** 139–158.

——, R. D. Farley, and H. D. Orville, 1983: Bulk parameterization of the snow field in a cloud model. *J. Climate Appl. Meteor.,* **22,** 1065–1092.

——, T.-A. Wang, and R. P. Weglarz, 1993: Interaction between gravity waves and cold air outflows in a stably stratified uniform flow. *J. Atmos. Sci.,* **50,** 3790–3816.

——, R. L. Deal, and M. S. Kulie, 1998: Mechanisms of cell regeneration, development, and propagation within a two-dimensional multicell storm. *J. Atmos. Sci.,* **55,** 1867–1886.

——, S. Chiao, T.-A. Wang, M. L. Kaplan, and R. P. Weglarz,

2001a: Some common ingredients for heavy orographic rainfall. *Wea. Forecasting,* **16,** 633–660.

——, J. A. Thurman, and S. Chiao, 2001b: Influence of synoptic and mesoscale environments on heavy orographic rainfall associated with MAP IOP2B and IOP8. *MAP Newsletter*, No. 15, 72–75. [Available online at http://www.map.ethz.ch/newsletter15.htm.]

Michalakes, J., S.-H. Chen, J. Dudhia, L. Hart, J. Klemp, J. Middlecoff, and W. Skamarock, 2001: Development of a next generation regional weather research and forecast model. *Developments in Teracomputing: Proceedings of the Ninth ECMWF Workshop on the Use of High Performance Computing in Meteorology*, W. Zwieflhofer and N. Kreitz, Eds., World Scientific, 269–276.

Miglietta, M. M., and A. Buzzi, 2001: A numerical study of moist stratified flows over isolated topography. *Tellus,* **53A,** 481–499.

Raymond, D. J., and R. Rotunno, 1989: Responses of a stably stratified flow to cooling. *J. Atmos. Sci.,* **46,** 2830–2837.

Rotunno, R., and R. Ferretti, 2001: Mechanisms of intense Alpine rainfall. *J. Atmos. Sci.,* **58,** 1732–1749.

Rutledge, S. A., and P. V. Hobbs, 1984: The mesoscale and microscale structure and organization of clouds and precipitation in midlatitude cyclones. XII: A diagnostic modeling study of precipitation development in narrow cloud-frontal rainbands. *J. Atmos. Sci.,* **41,** 2949–2972.

Schlesinger, R. E., 1978: A three-dimensional numerical model of an isolated thunderstorm: Part I. Comparative experiments for variable ambient wind shear. *J. Atmos. Sci.,* **35,** 690–713.

Schneidereit, M., and C. Schär, 2000: Idealised numerical experiments of Alpine flow regimes and southside precipitation events. *Meteor. Atmos. Phys.,* **72,** 233–250.

Skamarock, W. C., J. B. Klemp, and J. Dudhia, 2001: Prototypes for the WRF (Weather Research and Forecast) model. Preprints, *Ninth Conf. on Mesoscale Processes*, Fort Lauderdale, FL, Amer. Meteor. Soc., J11–J15.

Smith, R. B., 1979: The influence of mountains on the atmosphere. *Advances in Geophysics*, Vol. 21, Academic Press, 87–230.

——, 1985: On severe downslope winds. *J. Atmos. Sci.,* **42,** 2597–2603.

——, 1989: Hydrostatic airflow over mountains. *Advances in Geophysics*, Vol. 31, Academic Press, 1–41.

——, 2003: A linear upslope-time-delay model for orographic precipitation. *J. Hydrol.,* **282,** 2–9.

Stein, J., 2004: Exploration of some convective regimes over the Alpine orography. *Quart. J. Roy. Meteor. Soc.,* **130,** 481–502.

Thorpe, A., M. J. Miller, and M. W. Moncrieff, 1980: Dynamical models of two-dimensional downdraughts. *Quart. J. Roy. Meteor. Soc.,* **106,** 463–484.

Wicker, L. J., and W. C. Skamarock, 2002: Time-splitting methods for elastic models using forward time schemes. *Mon. Wea. Rev.,* **130,** 2088–2097.

Yang, M.-J., and R. A. Houze Jr., 1995: Multicell squall line structure as a manifestation of vertically trapped gravity waves. *Mon. Wea. Rev.,* **123,** 641–660.